ACS central science

http://pubs.acs.org/journal/acscii

Research Article

Polymersomes Decorated with the SARS-CoV-2 Spike Protein Receptor-Binding Domain Elicit Robust Humoral and Cellular Immunity

Lisa R. Volpatti,[¶] Rachel P. Wallace,[¶] Shijie Cao,[¶] Michal M. Raczy,[¶] Ruyi Wang,[¶] Laura T. Gray, Aaron T. Alpar, Priscilla S. Briquez, Nikolaos Mitrousis, Tiffany M. Marchell, Maria Stella Sasso, Mindy Nguyen, Aslan Mansurov, Erica Budina, Ani Solanki, Elyse A. Watkins, Mathew R. Schnorenberg, Andrew C. Tremain, Joseph W. Reda, Vlad Nicolaescu, Kevin Furlong, Steve Dvorkin, Shann S. Yu, Balaji Manicassamy, James L. LaBelle, Matthew V. Tirrell, Glenn Randall, Marcin Kwissa, Melody A. Swartz,* and Jeffrey A. Hubbell*

Cite This: *ACS Cent. Sci.* 2021, 7, 1368−1380

Read Online

ACCESS | Metrics & More | Article Recommendations | Supporting Information

ABSTRACT: The COVID-19 pandemic underscores the need for rapid, safe, and effective vaccines. In contrast to some traditional vaccines, nanoparticle-based subunit vaccines are particularly efficient in trafficking antigens to lymph nodes, where they induce potent immune cell activation. Here, we developed a strategy to decorate the surface of oxidation-sensitive polymersomes with multiple copies of the SARS-CoV-2 spike protein receptor-binding domain (RBD) to mimic the physical form of a virus particle. We evaluated the vaccination efficacy of these surface-decorated polymersomes (RBD_{surf}) in mice compared to RBD-encapsulated polymersomes (RBD_{encap}) and unformulated RBD (RBD_{free}), using monophosphoryl-lipid-A-encapsulated polymersomes (MPLA PS) as an adjuvant. While all three groups produced high titers of RBD-specific IgG, only RBD_{surf} elicited a neutralizing antibody response to SARS-CoV-2 comparable to that of human convalescent plasma. Moreover, RBD_{surf} was the only group to significantly increase the proportion of RBD-specific germinal center B cells in the vaccination-site draining lymph nodes. Both RBD_{surf} and RBD_{encap} drove similarly robust $CD4^+$ and $CD8^+$ T cell responses that produced multiple Th1-type cytokines. We conclude that a multivalent surface display of spike RBD on polymersomes promotes a potent neutralizing antibody response to SARS-CoV-2, while both antigen formulations promote robust T cell immunity.

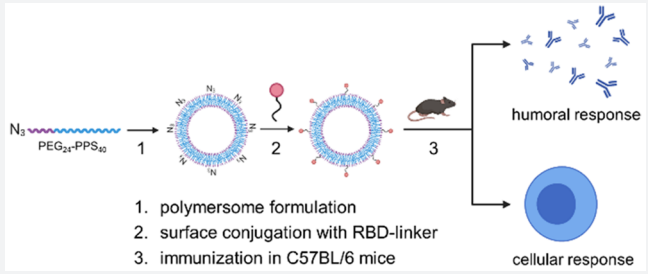

INTRODUCTION

COVID-19, the disease caused by the novel coronavirus SARS-CoV-2, emerged in late 2019 and was declared a pandemic by the World Health Organization in March 2020. Since its emergence, researchers across the world have sought to rapidly develop vaccine candidates, some of which have received Emergency Use Authorization by the U.S. Food and Drug Administration.[1,2] While the first vaccines that entered the clinic were based on nucleic acid technologies, subunit vaccines are gaining attention and have also shown promise in clinical trials.[3,4] The primary antigens used in preclinical and clinical vaccine candidates are the spike protein and its constituent receptor-binding domain (RBD). The RBD of the spike protein binds to the ACE-2 receptor on host cell surfaces, enabling viral entry into host cells.[5,6]

Several highly potent neutralizing antibodies have been isolated that target RBD and prevent viral binding and uptake, making it an attractive vaccine target.[7−10] Since RBD is smaller and more stable than the full homotrimeric spike fusion protein, it is also advantageous from a manufacturing and distribution perspective.[11] However, RBD has been shown to have lower immunogenicity than the full spike protein or its RBD-containing S1 domain.[12,13] Materials science and engineering approaches, particularly strategies involving nanotechnology, may improve RBD immunogenicity and thus aid in the development of next-generation vaccines.[14−16] Indeed, several approaches of self-assembling RBD into virus-like particles have resulted in potent neutralizing antibody responses.[17−20]

Received: May 18, 2021
Published: July 21, 2021

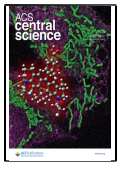

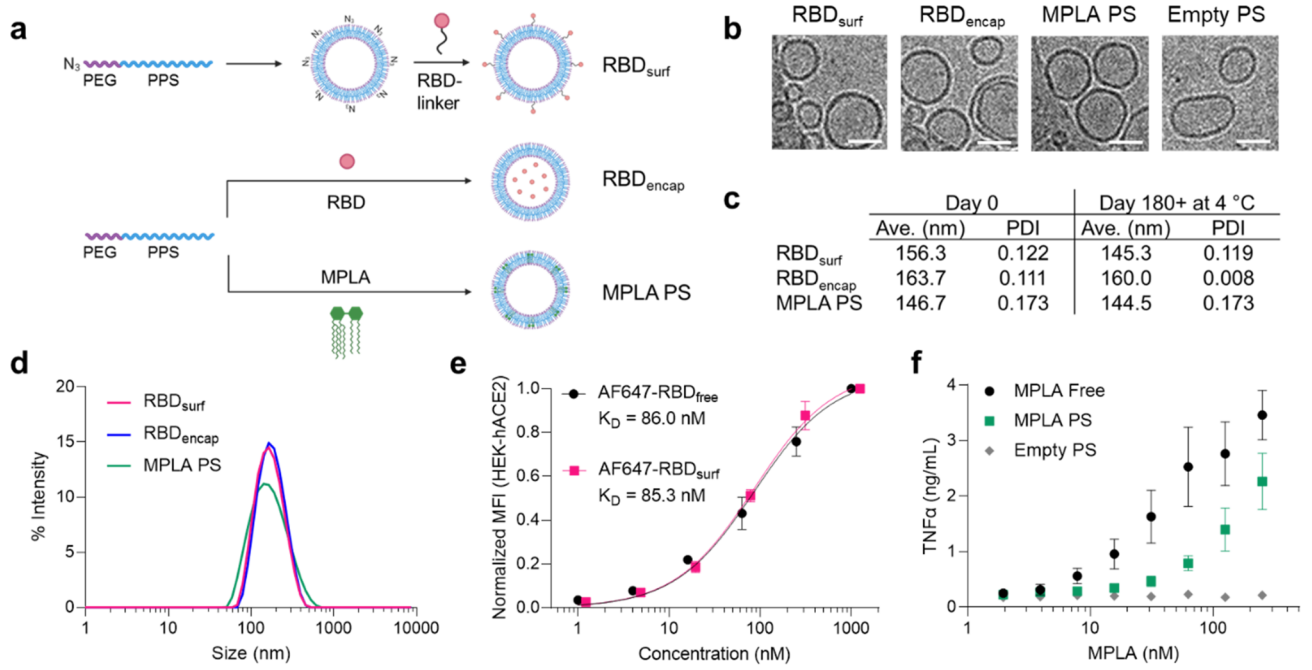

Figure 1. RBD and MPLA are formulated into stable, biologically active polymersomes (PS). (a) Schematic of formulation of PS. RBD was conjugated to the surface (RBD_{surf}) or encapsulated inside (RBD_{encap}) of PS, and MPLA was encapsulated in the vesicle membrane (MPLA PS) due to its hydrophobicity. (b) Representative cryo-electron microscopy images of PS, depicting vesicle structure. Scale = 50 nm. (c) Size and polydispersity index (PDI) from dynamic light scattering (DLS) measurements of PS upon formulation and after >180 days at 4 °C. (d) Representative DLS curves of PS. (e) Normalized mean fluorescence intensity (MFI) of AF647 conjugated to free RBD or RBD_{surf} by flow cytometry showing concentration-dependent binding to HEK-293 cells that express human ACE-2 (HEK-hACE2). Nonlinear regression was used to model data assuming specific binding to one site to determine equilibrium dissociation constants (K_D). (f) Dose-dependent secretion of TNFα from cultured murine bone-marrow-derived dendritic cells (BMDCs) stimulated by free MPLA, MPLA PS, or empty PS. Data represent mean ± SD for n = 2 (e) or 3 (f) replicates.

To offer robust protection from infection, cellular in addition to humoral responses are needed.[21−23] Almost all convalescent individuals show T cell immunity, and the majority have both $CD4^+$ and $CD8^+$ SARS-CoV-2-specific T cells.[24−27] Conversely, severe disease is associated with lymphopenia and reduced T cell function.[28−30] Furthermore, T cell immunity may be more durable than humoral responses, and T cells are expected to play an important role in immune memory.[23,28,31] Therefore, the goals of this study were to improve both humoral and cellular immunogenicity of RBD and compare the efficacy of engineered nanoparticle formulations in order to inform the design of next-generation nanovaccines.

We have previously reported the development of polymersomes (PS) that self-assemble from the oxidation-responsive block copolymer poly(ethylene glycol)-*bl*-poly(propylene sulfide) (PEG−PPS)[32] and shown their efficacy in delivering antigen and adjuvant to dendritic cell endosomes.[33] In endolysosomal compartments, the PPS block becomes oxidized, which initiates the restructuring of the PS into micelles and concurrent release of encapsulated payload.[33,34] These vaccine nanocarriers have been shown to activate dendritic cells, induce robust T cell immunity, and elicit high antibody titers with broad epitope coverage.[33,35,36]

In this study, we hypothesized that we could further improve the humoral responses elicited by PS while retaining their ability to induce T cell immunity by engineering them to mimic the physical form of a viral particle through multivalent surface display of antigen. We envisaged that multivalent surface display of RBD would result in enhanced cross-linking and clustering of B cell receptors (BCRs) and subsequent production of neutralizing antibodies. As such, we developed and evaluated PS displaying surface-bound RBD (RBD_{surf}) and PS encapsulating RBD (RBD_{encap}) adjuvanted with monophosphoryl-lipid-A-encapsulated PS (MPLA PS). MPLA was chosen as an adjuvant due to its hydrophobicity and ability to be encapsulated within the PPS-rich shell of the polymersomes without affecting antigen loading in future single-particle vaccines. Furthermore, as MPLA has been combined with aluminum hydroxide to prolong its retention as a clinical adjuvant,[37] we hypothesized that its incorporation into PS would similarly increase its efficacy. Here, we show that mice vaccinated with RBD_{surf} in combination with MPLA PS in a prime-boost schedule develop high titers of SARS-CoV-2-neutralizing antibodies with robust germinal center responses as well as $CD4^+$ and $CD8^+$ T cell immunity, thus meeting our design criteria.

RESULTS

Formulated Polymersomes Exhibit Long-Term Stability and *In Vitro* Activity. Having previously encapsulated antigen into PS as nanovaccines,[33] here we developed a conjugation strategy to attach antigens to their surface. To create a modular platform that could be generalized to virtually any antigen, we synthesized N_3−PEG−PPS (Figure S1), which, when formulated into PS, yields particles displaying clickable surface moieties (Figure 1a). Upon the addition of RBD conjugated to a DBCO-containing linker, we generated PS decorated with RBD (RBD_{surf}, Figure S2). We also synthesized PEG−PPS (Figure S3) and formulated PS

https://doi.org/10.1021/acscentsci.1c00596
ACS Cent. Sci. 2021, 7, 1368−1380

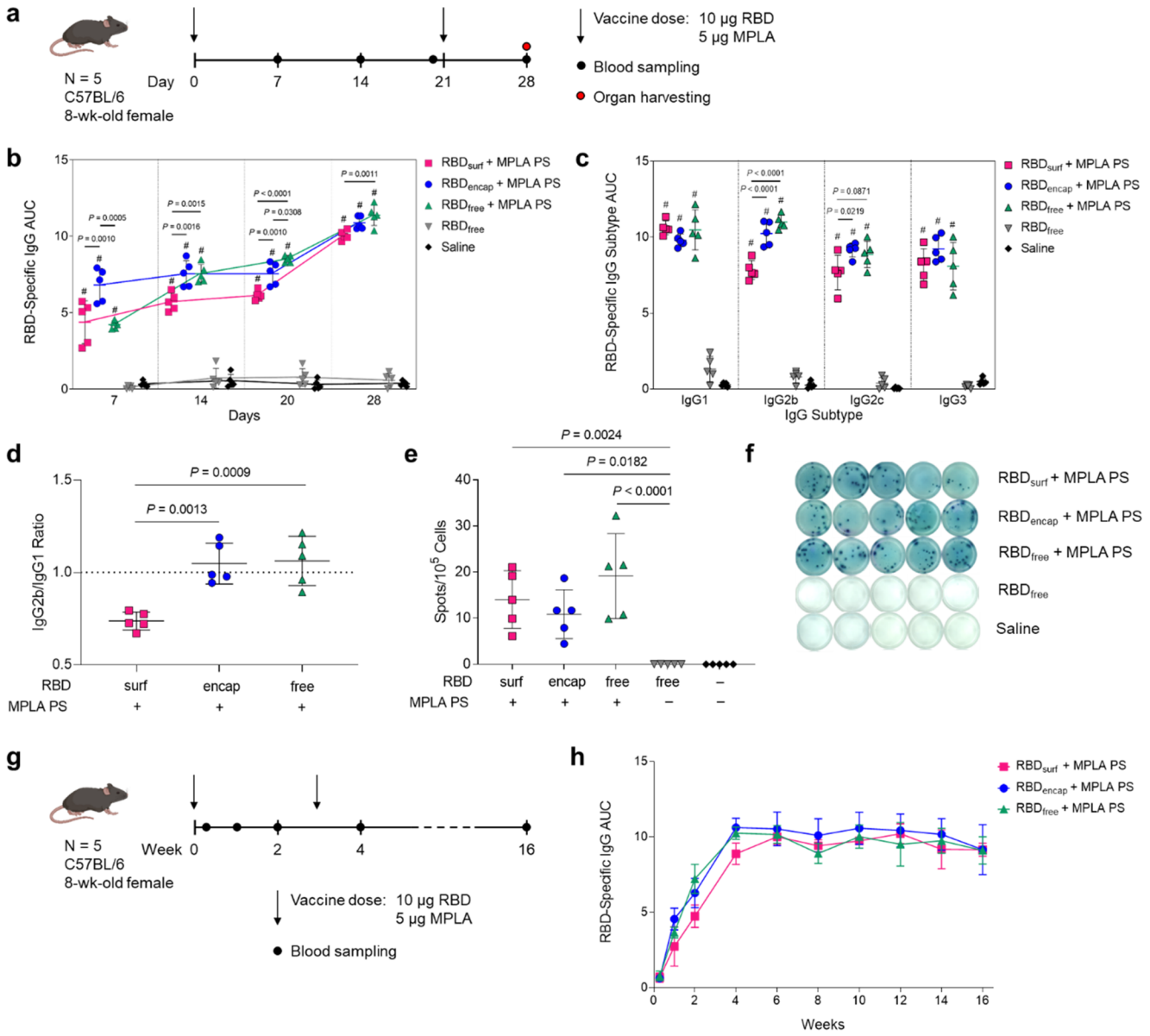

Figure 2. High levels of RBD-specific IgG antibodies are produced upon PS vaccination. (a) Vaccination schedule consisting of a priming dose followed by a booster 3 weeks later. (b) Total RBD-specific IgG antibodies over time reported as the area under the log-transformed curve (AUC) of absorbance vs dilution. (c) Comparison of RBD-specific IgG isotypes (IgG1, IgG2b, IgG2c, IgG3) on day 28. (d) Ratio of AUCs of IgG2b/IgG1 isotypes. (e) Quantification of RBD-specific IgG^+ antibody secreting cells by ELISpot of splenocytes (Dunn's post-test compared to unadjuvanted RBD_{free}). (f) Representative ELISpot wells from (e). Data plotted as mean ± SD and represent 1 of 2 experiments with $n = 5$ mice each. Symbols represent individual mice. (g) Vaccine and blood sampling schedule of long-term kinetics study. (h) Total RBD-specific IgG antibodies over time for the vaccination schedule in (g). Data represent mean ± SD for $n = 5$ mice. Comparisons were made using one-way ANOVA with Tukey's post-test unless stated otherwise. # $P < 0.0001$ compared to unadjuvanted RBD_{free}.

encapsulating RBD (RBD_{encap}) or adjuvant (MPLA PS, Figure 1a). The loading capacities of RBD_{surf} and RBD_{encap} were 1.57 and 1.75%, respectively, comparable to previous reports of encapsulated ovalbumin,[33,35] while the loading capacity of MPLA PS was 6.46% (Table S1). We confirmed the vesicular structure of PS through cryo-electron microscopy (cryoEM) and demonstrated that the different formulations have similar sizes and morphologies (Figures 1b and S4). According to dynamic light scattering (DLS) measurements, the average PS diameter is around 150 nm (Figure 1c,d), which is comparable to the reported size of SARS-CoV-2 particles (60−140 nm).[38] The polydispersity index (PDI) of each formulation was less than 0.2, indicative of a relatively homogeneous population of nanovesicles. As indicated by their consistent size and PDI, in addition to the absence of free RBD released into solution, PS remain stable at 4 °C for at least 180 days, which can be beneficial for distribution and shelf life considerations (Figures 1c and S5).

We next characterized the biological activity of the PS formulations *in vitro*. To confirm that RBD structure is not substantially altered upon conjugation to the PS surface, we quantified its ability to bind to HEK-293 cells that express human ACE-2 (HEK-hACE2, Figure 1e). The normalized mean fluorescence intensity (MFI) versus RBD concentration curves were used to calculate the equilibrium dissociation constants (K_D) for free RBD and RBD_{surf} conjugated to AF647

https://doi.org/10.1021/acscentsci.1c00596
ACS Cent. Sci. 2021, 7, 1368−1380

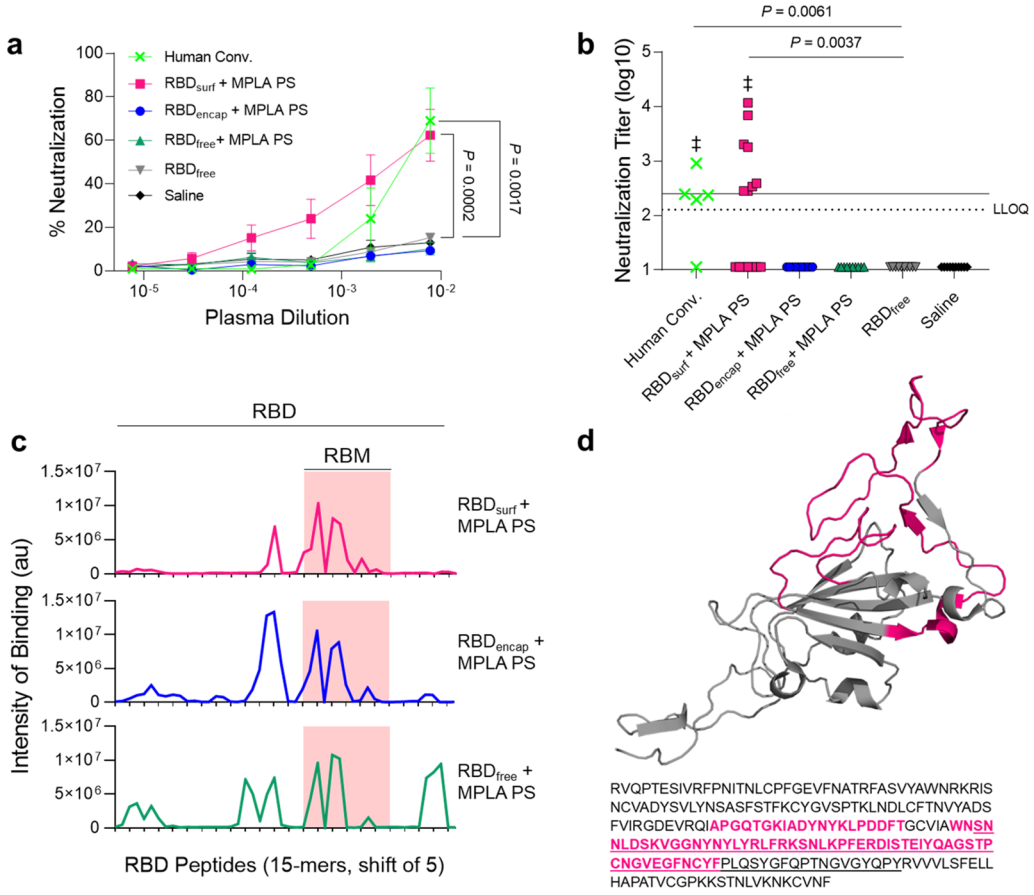

Figure 3. Antibodies induced by vaccination with RBD_{surf} + MPLA PS are neutralizing and localized to the receptor-binding motif. (a) Plasma from mice 1 week postboost was tested for its ability to neutralize SARS-CoV-2 infection of Vero E6 cells *in vitro*. Percent neutralization for multiple plasma dilutions normalized to cells without virus (100%) or without plasma (0%). Data plotted as mean ± SEM for $n = 5$ human convalescent samples (human conv.) or 10−15 mice. Comparisons to unadjuvanted RBD_{free} were made for lowest dilution ($10^{-2.11}$) using one-way ANOVA with Dunnett's post-test. (b) Virus neutralization titers, representing the plasma dilution at which 50% of SARS-CoV-2-mediated cell death is neutralized. Dashed line: lower limit of quantification (LLOQ = 2.11). For values below the LLOQ, LLOQ/2 values were plotted. Solid line: FDA recommendation for "high titer" classification (=2.40). Comparisons were made using a Kruskal−Wallis nonparametric test with Dunn's post-test or a Wilcoxon signed rank test (‡ ns, $P > 0.05$ compared to hypothetical value of 2.40). Symbols represent individual mice. (c) Pooled plasma was then tested for antibody binding to linear epitopes using overlapping 15-amino-acid peptides with 5-amino-acid offsets, spanning the entire RBD sequence. The *x*-axis represents sequential peptide number within the RBD amino acid sequence showing the position of the receptor-binding motif (RBM), and the *y*-axis represents average luminescence for each peptide epitope. (d) 3D structure and amino acid sequence of RBD with the RBM underlined and main peptide sequences recognized by mouse plasma highlighted in pink (Protein Data Bank Entry 7DDD).

($AF647\text{-}RBD_{free}$ and $AF647\text{-}RBD_{surf}$, respectively). The curves and K_D values are in excellent agreement, indicating that surface conjugation to PS does not impact ACE-2 binding of RBD. Empty PS conjugated to AF647 did not bind to HEK-hACE2, and neither PS formulation bound to HEK-293 cells lacking hACE-2 (Figure S6).

Next, we confirmed that MPLA retained its ability to serve as a TLR4 agonist upon formulation in PS with a HEK-Blue TLR4 reporter cell line (Figure S7). To further validate MPLA PS activity in a more physiologically relevant model, we stimulated murine bone-marrow-derived dendritic cells (BMDCs) with free MPLA, MPLA PS, or empty PS, and we measured the subsequent secretion of the proinflammatory cytokines TNFα, IL-6, IL-1α, and IL-1β (Figures 1f and S8). For each cytokine, there was a dose-dependent increase in secretion for free MPLA and MPLA PS with only background levels of secretion for empty PS, indicating that MPLA PS successfully activated antigen presenting cells (APCs) *in vitro*. Thus, we successfully synthesized two RBD formulations of PS in addition to MPLA PS and showed that they are homogeneous vesicular structures with long-term stability and *in vitro* biological activity.

All Adjuvanted Formulations Elicit RBD-Specific IgG Responses. Having confirmed that antigen- and adjuvant-loaded PS exhibit their expected bioactivity *in vitro*, we next evaluated their ability to enhance humoral and cellular immunity in 8-week-old, female C57BL/6 mice compared to RBD_{free}. We immunized mice via subcutaneous (s.c.) injection in the hocks in a prime-boost schedule 3 weeks apart and monitored antibody titers weekly (Figure 2a). The total RBD-specific IgG is represented by the area under the log-transformed ELISA absorbance curves (AUC), starting at a plasma dilution of 10^{-2} (see Methods, Figure S9). All adjuvanted groups had significant RBD-binding antibody responses within a week after their first dose, with RBD_{encap} stimulating the highest responses (Figure 2b). The antibody responses in adjuvanted groups either increased gradually or remained constant until a week after the booster, when the mean AUC increased 1.3- to 1.6-fold.

https://doi.org/10.1021/acscentsci.1c00596
ACS Cent. Sci. 2021, 7, 1368−1380

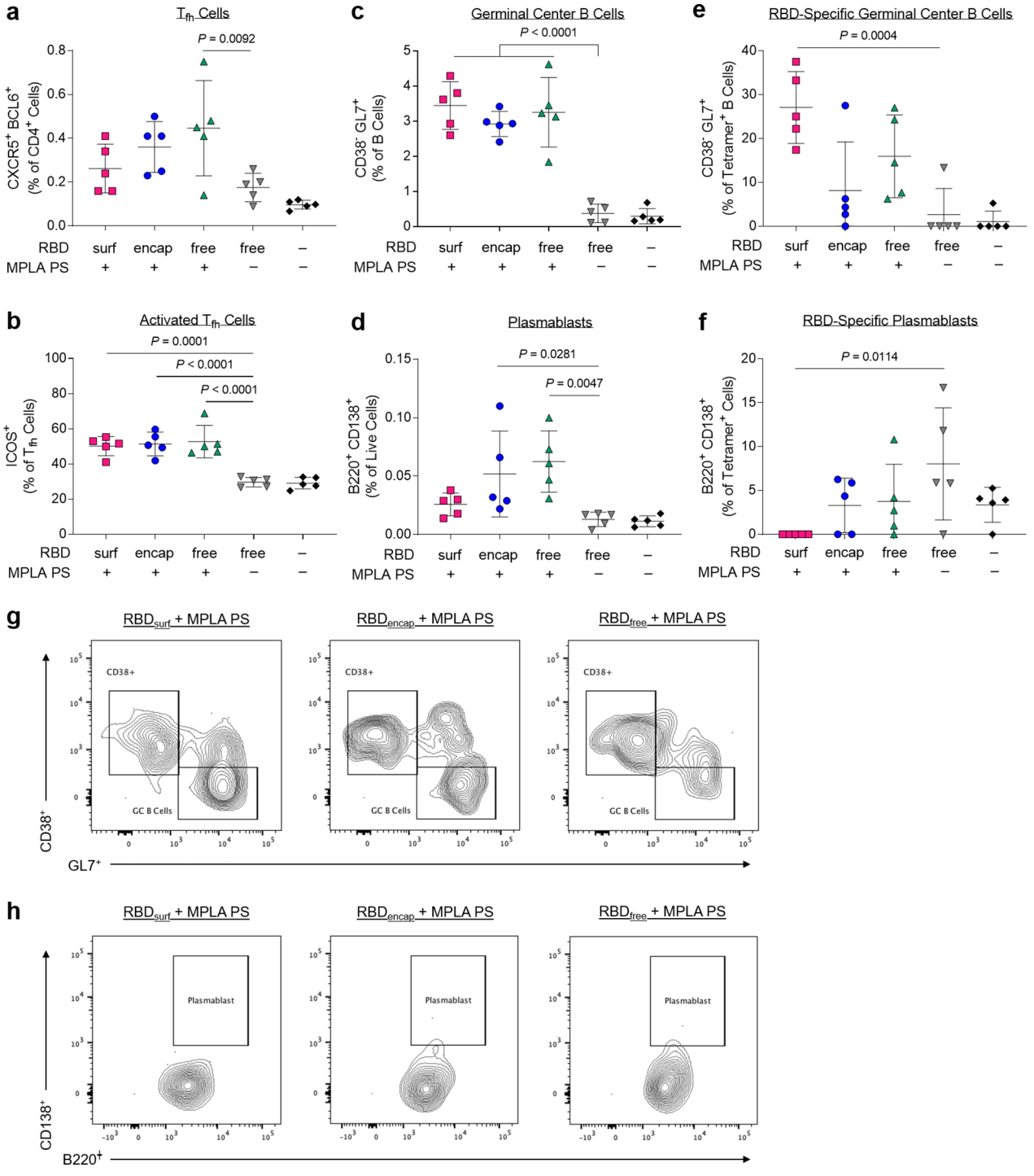

Figure 4. CD4$^+$ T follicular helper cells (T_{fh}) and B cells are activated by PS vaccine 1 week postboost in the injection site draining lymph nodes (dLN). (a) T_{fh} cells (CXCR5$^+$ BCL6$^+$) of vaccinated mice quantified via flow cytometry as a percent of live CD4$^+$ T cells. (b) Highly activated ICOS$^+$ T_{fh} cells quantified as percent of T_{fh} cells. (c) Germinal center B cells (CD38$^-$ GL7$^+$) quantified as a percentage of total B cells (B220$^+$ CD19$^+$). (d) Plasmablasts (B220$^+$ CD138$^+$) quantified as a percentage of total dLN cells. (e) Germinal center B cells quantified as a percentage of RBD-specific B cells. (f) Plasmablasts quantified as a percentage of RBD-specific dLN cells. (g,h) Concatenated flow cytometry contour plots for n = 5 mice/group showing RBD-specific GC B cells (g) or plasmablasts (h). Data plotted as mean ± SD and represent 1 of 2 experiments with n = 5 mice each. Symbols represent individual mice. Comparisons to unadjuvanted RBD_{free} were made using one-way ANOVA with Dunn's post-test.

In order to explore the humoral response in further detail, we then evaluated IgG subtypes of induced antibodies at the study end point (day 28, 1 week postboost). While plasma antibody levels of all adjuvanted groups were similar for IgG1 and IgG3, RBD_{surf} elicited significantly lower IgG2b and IgG2c antibody responses (Figure 2c). The ratio of IgG2b/IgG1 was then taken as an indication of a Th1/Th2-mediated response.[39] While RBD_{encap} and RBD_{free} + MPLA PS have a ratio of around 1, indicating a balanced Th1/Th2 response, RBD_{surf} shows a lower ratio of IgG2b to IgG1, indicating a slightly Th2-skewed response (Figure 2d). Since IgA is important for combating respiratory viruses at the mucosal

https://doi.org/10.1021/acscentsci.1c00596
ACS Cent. Sci. 2021, 7, 1368−1380

sites, we also measured plasma levels of RBD-specific IgA antibodies.[40,41] Although we did not expect high titers of circulating IgA from an s.c. administered vaccine, there were detectable anti-RBD IgA antibodies in all adjuvanted groups, which were significantly higher than the background-level responses elicited by unadjuvanted RBD_{free} (Figure S10).

We next aimed to determine whether the presence of RBD-specific antibodies from the priming dose affects the drainage of RBD_{surf} to the lymph nodes during the booster. To accomplish this goal, we compared the accumulation of fluorescently labeled RBD_{surf} in the lymph nodes of mice that had been previously immunized with RBD_{surf} or saline in a prime-boost schedule and had mean RBD-specific IgG AUCs of 9.9 and 0.23, respectively. AF647-RBD_{surf} and MPLA PS were injected s.c. in the hocks, and the brachial and popliteal draining lymph nodes were collected and fluorescently imaged 24 h later (Figure S11a). There was no significant difference in the total radiant efficiency of the lymph nodes between the preimmunized and saline control groups, indicating that the presence of antibodies does not substantially affect PS accumulation in the lymph nodes at this time point (Figure S11b).

Next, to determine if the higher antibody responses of adjuvanted groups stemmed from an expanded number of RBD-specific antibody secreting cells (ASCs), we performed an *ex vivo* RBD enzyme-linked immunosorbent spot (ELISpot) assay with splenocytes harvested 1 week postboost. All groups receiving adjuvanted RBD showed significantly higher RBD-specific IgG^+ ASCs compared to unadjuvanted RBD_{free}, consistent with plasma antibody levels (Figure 2e,f).

Finally, we evaluated the kinetics and durability of the humoral response to demonstrate the persistence of elicited antibodies (Figure 2g). The RBD-specific IgG AUC for all adjuvanted groups increased until 1 week postboost (week 4) and then remained constant over the subsequent 12 weeks, indicating that the antibody responses stimulated by these vaccine formulations persist for at least 4 months in mice after the initial dose. The results of this later experiment correlate with the two experiments performed according to the timeline in Figure 2a, suggesting that not only are the PS stable upon storage at 4 °C but also maintain their activity. Specifically, our data suggest RBD_{surf}, RBD_{encap}, and MPLA PS remain active for at least 4, 6, and 10 months, respectively. Taken together, MPLA PS-adjuvanted RBD_{surf}, RBD_{encap}, and RBD_{free} all stimulated persistent anti-RBD antibodies with increased frequencies of splenic RBD-specific ASCs while maintaining their activity upon storage at 4 °C for extended durations.

RBD-Surface-Decorated Polymersomes, but Not RBD-Encapsulated Polymersomes, Induce Neutralizing Antibodies. After analyzing the quantity of RBD-specific antibodies produced by the vaccine candidates, we next sought to determine their neutralizing capacity and breadth of epitope recognition. Neutralizing antibodies were assessed against SARS-CoV-2 infection of Vero E6 cells *in vitro*. Although all adjuvanted groups elicited similarly high titers of RBD-binding IgG antibodies (10^5–10^7, Figure S12a), only RBD_{surf} neutralized the virus to a greater extent than unadjuvanted RBD_{free} at a plasma dilution of $10^{-2.11}$ (lower limit of quantification, Figure 3a). We then quantified the virus neutralization titer (VNT) as the dilution at which 50% of SARS-CoV-2-mediated cell death is neutralized. There was no significant difference between VNTs of human convalescent plasma and RBD_{surf} plasma, and both groups induced higher VNTs compared to unadjuvanted RBD_{free} (Figure 3b). Furthermore, the median VNT elicited by RBD_{surf} was 2.45, which falls within the FDA classification of "high titer" for convalescent plasma therapy (>2.40).[42] To ensure reproducibility, the neutralization assay was repeated with 3 different cohorts of $n = 5$ mice each, and no significant differences were observed between the resulting VNTs (Figure S12b).

We next aimed to determine whether differences in neutralizing ability resulted from the epitope recognition breadth elicited by each vaccine formulation. To test this, we mapped the epitopes recognized by vaccine-elicited antibodies using a linear peptide array from the full-length RBD sequence. While IgG antibodies elicited by RBD_{surf} primarily recognized linear epitopes concentrated within the receptor-binding motif of RBD (RBM; aa 438–508), RBD_{encap} and RBD_{free} + MPLA PS exhibited broader linear epitope diversity (Figures 3c,d and S13). Within RBD, the RBM is particularly critical for interacting with ACE-2, so antibodies specific for this region may have potent neutralizing potential.[43,44]

Because RBD_{surf} appeared to offer the advantage of improved neutralizing activity while RBD_{encap} offered epitope diversity, we asked if coadministration would synergize to further enhance protection. To test this, we mixed RBD_{surf} and RBD_{encap} (with the total RBD dose remaining constant) with MPLA PS and treated mice using the same vaccination schedule. As an additional control, we also investigated the humoral response of RBD_{free} adjuvanted with free MPLA. While both groups produced high RBD-specific IgG AUCs, neither exhibited neutralizing potential against the SARS-CoV-2 virus above background levels (Figure S14a,b). Analysis of the peptide arrays for these groups shows the presence of high-intensity-binding antibodies outside of the RBM (Figure S14c).

In summary, while all adjuvanted groups elicit high titers of RBD-specific antibodies, only RBD_{surf} generated neutralizing antibodies against SARS-CoV-2 at titers comparable to human convalescent plasma. Additionally, these antibodies uniquely bound to linear epitopes localized within the RBM, while all other groups produced antibodies with greater epitope breadth.

All Adjuvanted Formulations Increase T_{fh} and B Cell Activation in the dLN. Given the differences in antibody responses and neutralizing activity elicited by RBD_{surf} versus RBD_{encap} vaccination, we further investigated the phenotypes of the B and T cells involved in the initiation of the humoral immune response. All adjuvanted groups showed trends of higher frequencies of T follicular helper cells (T_{fh}; $CD4^+$ $CXCR5^+$ $BCL6^+$) in the injection site draining lymph nodes (dLNs) 1 week postboost compared to unadjuvanted RBD_{free} (Figures 4a and S15), although differences were only statistically significant for RBD_{free} + MPLA PS. Interestingly, a greater percentage of T_{fh} cells in all adjuvanted groups highly upregulated expression of ICOS, a costimulatory receptor important in T_{fh} activation and maintenance (Figure 4b).[45]

Following activation by T_{fh} cells, naïve B cells can either undergo a germinal center (GC)-dependent response, in which they become GC B cells and undergo cycles of class-switching and somatic hypermutation (SHM) before differentiation into long-lived plasma cells and class-switched memory B cells, or they can differentiate into short-lived plasmablasts or IgM memory cells in a GC-independent response.[46] A stronger GC response is valuable in vaccination, because it results in higher affinity and longer-lived antibody production.[47] Overall

https://doi.org/10.1021/acscentsci.1c00596
ACS Cent. Sci. 2021, 7, 1368–1380

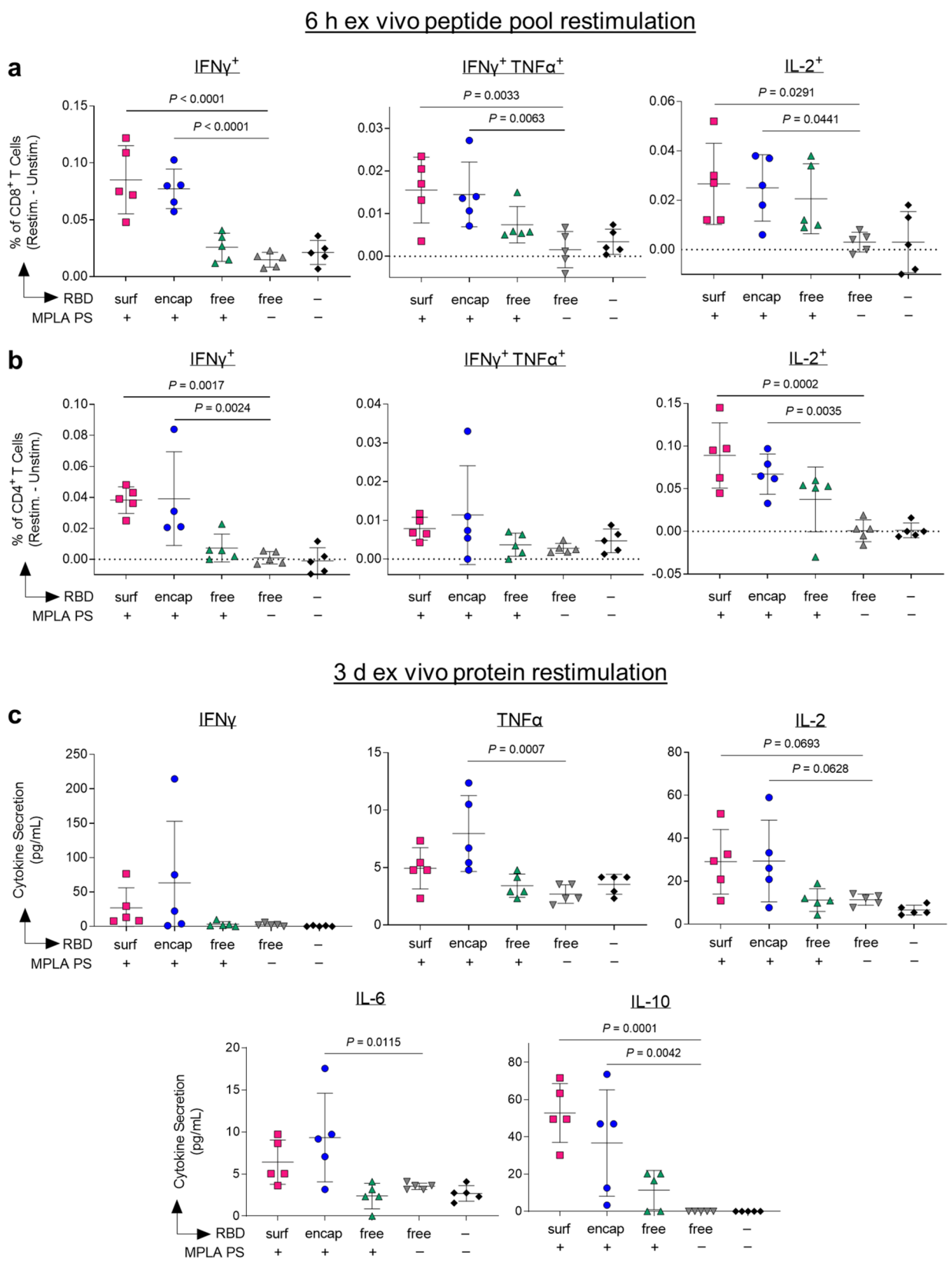

Figure 5. Vaccination with polymersome-formulated RBD improves antigen-specific T cell responses in mice. Cells isolated from dLN of PS-vaccinated mice 1 week postboost were restimulated *ex vivo* for 6 h with RBD peptide pools or 3 days with full RBD protein and analyzed by flow cytometry or multiplexed ELISA, respectively. (a,b) Percentages of cytokine-positive $CD8^+$ T cells (a) and $CD4^+$ T cells (b) in response to RBD peptide pools, subtracting unstimulated controls. (c) Proinflammatory cytokine levels in the supernatant measured after restimulation with whole RBD protein. Data plotted as mean ± SD and represent 1 of 2 experiments with $n = 5$ mice each. Symbols represent individual mice. Comparisons to unadjuvanted RBD_{free} were made using one-way ANOVA with Dunn's post-test.

https://doi.org/10.1021/acscentsci.1c00596
ACS Cent. Sci. 2021, 7, 1368−1380

frequencies of B cells ($CD19^+$ $B220^+$) were unaffected across groups, but there were significantly lower frequencies of naïve IgD^+ B cells in the adjuvanted groups compared to unadjuvanted RBD_{free} (Figures S16 and S17). All adjuvanted groups generated GC responses, characterized by increased frequencies of GC B cells ($CD38^-$ $GL7^+$) in the dLN compared to unadjuvanted RBD_{free} (Figure 4c). Both RBD_{encap} and RBD_{free} + MPLA PS formulations, but not RBD_{surf}, significantly increased the frequencies of plasmablasts ($B220^+$ $CD138^+$) in the dLN compared to unadjuvanted RBD_{free} (Figure 4d).

To determine the antigen specificity of the B cells, we developed a set of fluorescent RBD protein tetrameric probes. To ensure selectivity, B cells were considered RBD-specific if they were double-positive for both PE- and APC-conjugated RBD tetramers and negative for the nonspecific control protein tetramer (Figure S18). RBD_{free} + MPLA PS was the only formulation to significantly increase the frequency of RBD-specific B cells in the dLN (Figure S19). We next sought to further determine the phenotype of these RBD-specific B cells. RBD_{surf}, unlike the other adjuvanted formulations, led to a significantly higher fraction of RBD-specific B cells with GC B cell phenotype, suggesting a more robust GC response to RBD (Figure 4e). RBD_{surf} was also the only formulation with a significantly lower fraction of plasmablasts within the RBD-specific B cell subset compared to unadjuvanted RBD_{free} (Figure 4f). These differences are also visually apparent in pooled flow cytometry plots for RBD-specific GC B cells (Figure 4g) and plasmablasts (Figure 4h). In summary, all adjuvanted formulations of RBD increased activation of T_{fh} cells and GC B cells in the dLN, but within the RBD-specific B cell population, only RBD_{surf} generated a higher fraction of GC B cells and a lower fraction of plasmablasts.

Vaccination with Polymersome-Formulated RBD Generates RBD-Specific Th1 T Cell Responses. Having demonstrated that our PS vaccines can generate strong humoral responses, we next sought to determine their capacity to generate robust $CD8^+$ and $CD4^+$ T cell immunity. In order to assess the RBD-specific T cell response, we isolated cells from the dLNs of vaccinated mice 1 week postboost. Prior to intracellular staining, cells were restimulated with RBD peptide pools for 6 h. The RBD-specific response was quantified by subtracting the signal from cells incubated in media alone from those incubated with RBD peptide pools (Figure S20). Only PS-formulated RBD groups RBD_{surf} and RBD_{encap} generated significantly higher frequencies of $IFN\gamma^+$, bifunctional $IFN\gamma^+TNF\alpha^+$, and IL-2^+ $CD8^+$ T cells compared to unadjuvanted RBD_{free} (Figure 5a). Similar trends were seen in the $CD4^+$ T cell compartment. Treatment with RBD_{surf} and RBD_{encap} but not RBD_{free} + MPLA PS led to significantly higher frequencies of $IFN\gamma^+$ and IL-2^+ $CD4^+$ T cells, although the increase in bifunctional IFN $\gamma^+TNF\alpha^+$ was not statistically significant (Figure 5b). The production of these cytokines implies a Th1 T cell response, which has been correlated with less severe cases of SARS-CoV infection.[21]

For further validation of the cytokine response, cells from the dLN isolated from the same vaccinated mice were restimulated with full RBD protein *ex vivo* for 3 days, followed by quantification of cytokines in the supernatant. The RBD-specific response was quantified by subtracting unstimulated signal from stimulated signal as above. The levels of Th1-type cytokines detected were consistent with intracellular staining data. Levels of IFNγ and IL-2 were modestly but not significantly increased in the RBD_{surf} and RBD_{encap} groups compared to the RBD_{free} group, while cells from RBD_{encap}-treated mice secreted TNFα at significantly higher levels than unadjuvanted RBD_{free} (Figure 5c). RBD_{encap} also led to increased production of IL-6 and IL-10, which are pleiotropic cytokines known to be secreted during Th1 responses (Figure 5c).[48,49] Levels of secreted Th2-type cytokines were also measured. More IL-4 was produced in the supernatant of samples treated with RBD_{surf} and RBD_{encap} compared to RBD_{free}, albeit at an overall low concentration. There was no significant elevation of IL-5 secretion across any of the treatment groups compared to the saline control and no detectable levels of IL-13 in any sample (Figure S21). In summary, vaccination with RBD delivered via polymersome formulations generated stronger RBD-specific Th1-type $CD8^+$ and $CD4^+$ T cell responses than unadjuvanted RBD_{free}, while RBD_{free} + MPLA PS did not.

DISCUSSION

In this study, we developed antigen-decorated, oxidation-sensitive polymersomes that mimic virus particles as next-generation nanovaccines. While all adjuvanted formulations generated long-lived RBD-binding IgG responses, surface conjugation of antigen was necessary to generate neutralizing antibodies against SARS-CoV-2. More generally, this comparison of antigen formulation on the quality of immune response offers valuable insight into vaccine design, demonstrating the benefits of surface antigen display.

The differences in the immune responses elicited by the two PS antigen formulations, RBD_{surf} and RBD_{encap}, suggest that surface display of antigen leads to stronger GC responses, while PS-encapsulated antigen elicits more predominantly an extrafollicular response. Though RBD-specific GC B cells are present in the dLN after treatment with both formulations, a much higher percentage of the RBD-specific B cells recovered after vaccination with RBD_{surf} exhibited a GC B cell phenotype. This higher percentage could be due to the induction of higher numbers of RBD-specific GC B cells after vaccination with RBD_{surf} or an increase in their affinity, leading to easier detection via RBD protein tetramer staining. Both possibilities suggest a more robust GC response, as GC responses are necessary for an efficient SHM leading to increased B cell affinity.[50] Evidence for affinity maturation due to SHM also includes the relatively few epitopes on the RBD linear peptide array to which IgG from RBD_{surf}-treated groups were specific compared to the other adjuvanted groups. Clonal bursts in GC responses can lead to rapid expansion of high-affinity SHM variants and loss of overall clonal diversity.[51] A difference in the affinity of RBD-specific IgG generated by these vaccines may also explain the neutralization ability of the plasma after vaccination with RBD_{surf} but not RBD_{encap}. An interesting finding is that when RBD_{surf} and RBD_{encap} were codelivered, the resulting antibodies recognized a greater diversity of epitopes compared to RBD_{surf} alone and were also non-neutralizing. These data suggest that in the context of PS vaccines, epitope breadth and neutralization capacity may be mutually exclusive. Therefore, the decision of encapsulating antigen versus displaying it on the PS surface should be determined based on vaccine design criteria.

Further data that suggest that RBD_{encap} elicits a more extrafollicular response include the fast initial antibody response after priming by RBD_{encap}, which resulted in RBD-specific IgG AUC 1 week after the priming dose that was

https://doi.org/10.1021/acscentsci.1c00596
ACS Cent. Sci. 2021, 7, 1368−1380

significantly higher than that of RBD_{surf}. In an extrafollicular B cell response, B cells can differentiate immediately into plasmablasts and begin secreting antibodies after initial T cell help, whereas B cells that enter GCs delay the antibody response by several days.[46] The preferential differentiation into plasmablasts rather than GC B cells was also evident in the increased fraction of plasmablasts within the RBD-specific B cell population generated by RBD_{encap}. In vaccine development, the generation of robust GC reactions is typically preferable to extrafollicular responses, because GC formation usually results in higher affinity B cells, increased memory B cells, and increased long-lived plasma cells in the bone marrow.[46]

A potential rationale for these differences could be due to the multivalent display of RBD on RBD_{surf}. Multimeric structures have been associated with the induction of potent antibody responses due to BCR cross-linking in the presence of $CD4^+$ T cell help.[52] In our studies, RBD_{surf} most likely efficiently exposes for the BCR interaction the conformational epitopes of RBD reported to be targeted by neutralizing antibodies in plasma of convalescent or vaccinated individuals.[7−10] Furthermore, increased antigen valency has been shown to enhance early activation and proliferation of antigen-specific B cells as well as B cell accumulation at the T-B border, leading to increased differentiation of antigen-specific B cells into GC B cells and plasma cells.[53] Thus, the multimerization of RBD on the PS surface in addition to its increased availability to B cells led to an improved functional quality of humoral response compared to encapsulated or unformulated RBD.

The different formulations of RBD polymersomes likely access the follicular B cells via different mechanisms. In order for B cells to encounter their cognate antigen within the follicle, the antigen must first enter the subcapsular sinus of the lymph node and cross the subcapsular sinus barrier into the follicles. Particles 20−200 nm have been shown to gain ready access to lymphatics;[54] thus, both RBD_{surf} and RBD_{encap} particles likely enter into the draining lymph node with the afferent lymph into the subcapsular sinus after s.c. injection. Increased antigen exposure to B cells upon vaccination with RBD_{surf} may be due to protease activity in the sinus, which could cleave the surface-conjugated RBD from the larger particles, allowing the smaller proteins to diffuse into the follicular space, while the encapsulated RBD remains in the particle, which is too large to diffuse.[55] Alternatively, the PS may be taken up by the subcapsular sinus macrophages. These macrophages are nondegradative phagocytes and have been shown to uptake full particulate antigens and subsequently present them to B cells on the follicular side of the subcapsular sinus.[56] Presentation of antigen via subcapsular sinus macrophages is known to be increased for opsonized antigens via binding to complement receptor 3 and Fc receptor IIb.[57] Immune-complex formation on RBD_{surf} upon a boost due to circulating RBD-specific antibodies could explain an increase in GC responses compared to RBD_{encap}, which does not have exposed RBD-specific antibody epitopes. Cognate B cells in the follicle that encounter RBD_{surf} may become activated at the follicular border, avoiding the need to be trafficked into the B cell follicles.[58] RBD_{encap} particles, on the other hand, shield encapsulated RBD from B cell recognition and thus rely on uptake and degradation in APCs.

The type of immune response to SARS-CoV-2 may have important implications in how the infection is cleared and should be considered in vaccine design.[21] Less severe cases of SARS-CoV were associated with increased Th1-type cell responses.[59,60] In contrast, Th2-type responses were associated with increased pathology due to antibody-dependent enhancement, and several vaccine formulations against SARS-CoV showed signs of immunopathology due to Th2 cell-mediated eosinophil infiltration.[61,62] For our vaccine formulations, RBD_{encap} generated a IgG2b/IgG1 ratio around 1, suggesting a balance between type 1 and type 2 immunity, whereas RBD_{surf} generated a response with a slight IgG1 bias, suggestive of a more Th2-skewed response. The IgG2b/IgG1 ratio of RBD_{surf} is comparable to the IgG2a/c/IgG1 ratio reported for the mRNA-1273 SARS-CoV-2 vaccine although the mouse strain is different.[63] Additionally, the BNT162b mRNA vaccine elicited large numbers of $IgG1^+$ B cells in the spleen and LN of vaccinated mice.[64] Both of these mRNA vaccines elicit strong Th1 cytokine responses in addition to the production of IgG1 antibodies. Similarly, both RBD_{surf} and RBD_{encap} generated significant levels of the Th1-type cytokines IFNγ, TNFα, and IL-2, likely resulting from the use of MPLA as an adjuvant.[65] RBD_{surf} did not result in an increase in Th2-type cytokines upon restimulation compared to RBD_{encap}. Therefore, we conclude that RBD_{surf} promotes a balanced Th1/Th2 response, and the risk of adverse events related to Th2-type responses is low.

The PS-formulated RBD vaccines were able to generate stronger Th1-driven $CD4^+$ and $CD8^+$ T cell responses compared to RBD_{free}. We previously demonstrated that as an antigen delivery vehicle, PEG−PPS polymersomes improved cross-presentation to $CD8^+$ T cells.[33] This increased T cell response likely occurs as a result of both enhanced APC targeting and rapid endosomal antigen release.[33] APCs uptake membrane-impermeable nanocarriers such as PS more efficiently than other cell types due to their constitutive macropinocytosis.[66] Once endocytosed, PEG−PPS polymersomes require only a small amount of oxidation to release encapsulated antigen, and payload delivery to the cytosol is not restricted to endosomal compartments with reductive or acidic conditions.[33] Unlike antigen-encapsulated PS, however, acidification may be important for proteolytic degradation of RBD_{surf} and translocation to the cytosol.[67,68] Additionally, peptides derived from large antigen particles have been found to enter the cross-presentation pathways more efficiently than those derived from soluble antigens, which may provide rationale for the enhanced $CD8^+$ response of RBD_{surf}.[69] Therefore, antigen formulation using PS to improve T cell responses could be beneficial in the engineering of future vaccines against cancer or other infectious diseases for which T cell immune responses are thought to be necessary for protection, such as herpesviruses, human immunodeficiency virus, and hepatitis C virus.[70]

In summary, we have demonstrated that a polymersome-based antigen and adjuvant delivery system generates robust humoral immunity and neutralizing antibody titers as well as T cell responses against a key SARS-CoV-2 vaccine target, the RBD of the spike protein. This platform technology is amenable to a wide variety of antigens and formulated or soluble adjuvants. Once the type and dose of adjuvant has been optimized for a given application, a single particle could be used to deliver both antigen and adjuvant to APCs in the injection site draining lymph nodes. Additionally, multiple antigens, for example from different viruses or different strains or variants of the same virus, could be conjugated to the same

https://doi.org/10.1021/acscentsci.1c00596
ACS Cent. Sci. 2021, 7, 1368−1380

particle as a strategy to induce cross-reactive neutralizing antibodies.[20] Importantly, surface-decorated and antigen-encapsulated polymersomes remained stable and active at 4 °C for at least 6 and 4 months, respectively. Vaccines that exhibit long-term stability without requiring subzero temperatures will likely be important for widespread vaccine distribution, for example to rural populations or developing nations with poor cold chain networks. The evaluation of RBD-decorated polymersomes presented here could thus provide insight into the next generation of stable formulations of nanovaccines to combat the current COVID-19 pandemic as well as future viral outbreaks.

■ ASSOCIATED CONTENT

Supporting Information

The Supporting Information is available free of charge at https://pubs.acs.org/doi/10.1021/acscentsci.1c00596.

Methods, Figures S1−S21, Tables S1−S4 (PDF)

■ AUTHOR INFORMATION

Corresponding Authors

Melody A. Swartz − *Pritzker School of Molecular Engineering, Committee on Immunology, Ben May Department of Cancer Research, and Committee on Cancer Biology, University of Chicago, Chicago, Illinois 60637, United States*; Email: melodyswartz@uchicago.edu

Jeffrey A. Hubbell − *Pritzker School of Molecular Engineering, Committee on Immunology, and Committee on Cancer Biology, University of Chicago, Chicago, Illinois 60637, United States*; orcid.org/0000-0003-0276-5456; Email: jhubbell@uchicago.edu

Authors

Lisa R. Volpatti − *Pritzker School of Molecular Engineering, University of Chicago, Chicago, Illinois 60637, United States*; orcid.org/0000-0001-6197-0703

Rachel P. Wallace − *Pritzker School of Molecular Engineering, University of Chicago, Chicago, Illinois 60637, United States*

Shijie Cao − *Pritzker School of Molecular Engineering, University of Chicago, Chicago, Illinois 60637, United States*; orcid.org/0000-0002-9175-0813

Michal M. Raczy − *Pritzker School of Molecular Engineering, University of Chicago, Chicago, Illinois 60637, United States*

Ruyi Wang − *Pritzker School of Molecular Engineering, University of Chicago, Chicago, Illinois 60637, United States*

Laura T. Gray − *Pritzker School of Molecular Engineering, University of Chicago, Chicago, Illinois 60637, United States*

Aaron T. Alpar − *Pritzker School of Molecular Engineering, University of Chicago, Chicago, Illinois 60637, United States*

Priscilla S. Briquez − *Pritzker School of Molecular Engineering, University of Chicago, Chicago, Illinois 60637, United States*

Nikolaos Mitrousis − *Pritzker School of Molecular Engineering, University of Chicago, Chicago, Illinois 60637, United States*

Tiffany M. Marchell − *Committee on Immunology, University of Chicago, Chicago, Illinois 60637, United States*

Maria Stella Sasso − *Pritzker School of Molecular Engineering, University of Chicago, Chicago, Illinois 60637, United States*

Mindy Nguyen − *Pritzker School of Molecular Engineering, University of Chicago, Chicago, Illinois 60637, United States*

Aslan Mansurov − *Pritzker School of Molecular Engineering, University of Chicago, Chicago, Illinois 60637, United States*

Erica Budina − *Pritzker School of Molecular Engineering, University of Chicago, Chicago, Illinois 60637, United States*

Ani Solanki − *Animal Resources Center, University of Chicago, Chicago, Illinois 60637, United States*

Elyse A. Watkins − *Pritzker School of Molecular Engineering, University of Chicago, Chicago, Illinois 60637, United States*

Mathew R. Schnorenberg − *Pritzker School of Molecular Engineering, University of Chicago, Chicago, Illinois 60637, United States*

Andrew C. Tremain − *Committee on Immunology, University of Chicago, Chicago, Illinois 60637, United States*

Joseph W. Reda − *Pritzker School of Molecular Engineering, University of Chicago, Chicago, Illinois 60637, United States*

Vlad Nicolaescu − *Department of Microbiology, Howard T. Ricketts Laboratory, University of Chicago, Chicago, Illinois 60637, United States*

Kevin Furlong − *Department of Microbiology, Howard T. Ricketts Laboratory, University of Chicago, Chicago, Illinois 60637, United States*

Steve Dvorkin − *Department of Microbiology, Howard T. Ricketts Laboratory, University of Chicago, Chicago, Illinois 60637, United States*

Shann S. Yu − *Pritzker School of Molecular Engineering, University of Chicago, Chicago, Illinois 60637, United States*

Balaji Manicassamy − *Department of Microbiology and Immunology, University of Iowa, Iowa City, Iowa 52242, United States*

James L. LaBelle − *Department of Pediatrics, University of Chicago Comer Children's Hospital, Chicago, Illinois 60637, United States*; orcid.org/0000-0001-6776-4695

Matthew V. Tirrell − *Pritzker School of Molecular Engineering, University of Chicago, Chicago, Illinois 60637, United States; Materials Science Division, Argonne National Laboratory, Lemont, Illinois 60439, United States*; orcid.org/0000-0001-6185-119X

Glenn Randall − *Department of Microbiology, Howard T. Ricketts Laboratory, University of Chicago, Chicago, Illinois 60637, United States*

Marcin Kwissa − *Pritzker School of Molecular Engineering, University of Chicago, Chicago, Illinois 60637, United States*

Complete contact information is available at: https://pubs.acs.org/10.1021/acscentsci.1c00596

Author Contributions

¶L.R.V., R.P.W., S.C., M.M.R., and R.W. contributed equally to this work

Author Contributions

L.R.V., R.P.W., S.C., M.M.R., R.W., S.S.Y., M.K., M.A.S., and J.A.H. conceived the project and designed the research strategy. L.R.V., R.P.W., S.C., M.M.R., R.W., L.T.G., A.T.A., P.S.B., N.M., T.M.M., M.S.S., M.N., A.M., E.B., A.S., E.A.W., A.C.T., and J.W.R. performed experiments. L.R.V., R.P.W., S.C., M.M.R., A.T.A., P.S.B., T.M.M., and M.S.S. performed data analysis. P.S.B., V.N., K.F., S.D., and G.R. performed or advised on SARS-CoV-2 neutralization assays. M.R.S., J.L.L., and M.V.T. advised on surface modification of polymersomes. B.M. contributed the HEK-293-hACE2 cell line. L.R.V. and R.P.W. wrote the manuscript with contributions from S.C., S.S.Y., M.K., M.A.S., and J.A.H. All authors reviewed and approved the final version of the manuscript.

https://doi.org/10.1021/acscentsci.1c00596
ACS Cent. Sci. 2021, 7, 1368−1380

Notes

The authors declare the following competing financial interest(s): M.A.S. and J.A.H. have patents related to the polymersome technology and interests in LantaBio, which has licensed those patents.

■ ACKNOWLEDGMENTS

We are grateful for funding support through a pilot project grant from the Chicago Immunoengineering Innovation Center of the University of Chicago as well as the Chicago Biomedical Consortium COVID-19 Response Award (# CR-002) to M.A.S. In addition, a number of researchers were supported by fellowships via the NIH NHLBI (# T32-HL007605 to L.R.V.), Canadian Institutes of Health Research (#201910MFE-430736-73744 to N.M.), University of Chicago Comprehensive Cancer Center (Sigal Fellowship in Immuno-Oncology to N.M.), NIH NCI (# F30-CA221250 to M.R.S.), NIH NIGMS (# T32-GM007281 to M.R.S.), and NIH NIAID (# T32-AI007090 to T.M.M. and A.C.T.). We are grateful to the laboratory of Florian Krammer (Icahn School of Medicine at Mount Sinai, New York City, NY) for providing plasmids coding for the spike RBD, produced with support from the NIH NIAID (Contract # HHSN272201400008C). We are also grateful to the groups of Jesse Bloom (Fred Hutchinson Cancer Research Center, Seattle, WA) and Ali Ellebedy (Washington University School of Medicine, St. Louis, MO) for contributing reagents via the NIH NIAID BEI Resources repository. We acknowledge helpful discussions with Patrick C. Wilson, Jenna J. Guthmiller, Anne I. Sperling, and Aaron Esser-Kahn (University of Chicago, Chicago, IL) and with Robert Baker and David Boltz (Illinois Institute of Technology Research Institute, Chicago, IL) that were instrumental to experimental planning and model development. We acknowledge Suzana Gomes and Tera Lavoie for technical assistance. Parts of this work were carried out at the Cytometry and Antibody Technology Core Facility (Cancer Center Support Grant P30CA014599), the Soft Matter Characterization Facility, the Mass Spectrometry Facility (NSF instrumentation grant CHE-1048528), the Nuclear Magnetic Resonance Facility, the Advanced Electron Microscopy Facility (RRID:SCR_019198), and the Human Immunologic Monitoring Facility (RRID:SCR_017916) at the University of Chicago.

■ REFERENCES

(1) Le, T. T.; Cramer, J. P.; Chen, R.; Mayhew, S. Evolution of the COVID-19 vaccine development landscape. *Nat. Rev. Drug Discovery* **2020**, *19*, 667−668.

(2) Kyriakidis, N. C.; López-Cortés, A.; González, E. V.; Grimaldos, A. B.; Prado, E. O. SARS-CoV-2 vaccines strategies: a comprehensive review of phase 3 candidates. *npj Vaccines* **2021**, *6*, 28.

(3) Richmond, P.; Hatchuel, L.; Dong, M.; Ma, B.; Hu, B.; Smolenov, I.; Li, P.; Liang, P.; Han, H. H.; Liang, J.; Clemens, R. Safety and immunogenicity of S-Trimer (SCB-2019), a protein subunit vaccine candidate for COVID-19 in healthy adults: a phase 1, randomised, double-blind, placebo-controlled trial. *Lancet* **2021**, *397*, 682−694.

(4) Keech, C.; Albert, G.; Cho, I.; Robertson, A.; Reed, P.; Neal, S.; Plested, J. S.; Zhu, M.; Cloney-Clark, S.; Zhou, H.; et al. Phase 1−2 Trial of a SARS-CoV-2 Recombinant Spike Protein Nanoparticle Vaccine. *N. Engl. J. Med.* **2020**, *383*, 2320−2332.

(5) Zhou, P.; Yang, X.-L.; Wang, X.-G.; Hu, B.; Zhang, L.; Zhang, W.; Si, H.-R.; Zhu, Y.; Li, B.; Huang, C.-L.; et al. A pneumonia outbreak associated with a new coronavirus of probable bat origin. *Nature* **2020**, *579*, 270−273.

(6) Lan, J.; Ge, J.; Yu, J.; Shan, S.; Zhou, H.; Fan, S.; Zhang, Q.; Shi, X.; Wang, Q.; Zhang, L.; Wang, X.; et al. Structure of the SARS-CoV-2 spike receptor-binding domain bound to the ACE2 receptor. *Nature* **2020**, *581*, 215−220.

(7) Cao, Y.; Su, B.; Guo, X.; Sun, W.; Deng, Y.; Bao, L.; Zhu, Q.; Zhang, X.; Zheng, Y.; Geng, C.; et al. Potent Neutralizing Antibodies against SARS-CoV-2 Identified by High-Throughput Single-Cell Sequencing of Convalescent Patients' B Cells. *Cell* **2020**, *182*, 73−84.e16.

(8) Zost, S. J.; Gilchuk, P.; Case, J. B.; Binshtein, E.; Chen, R. E.; Nkolola, J. P.; Schäfer, A.; Reidy, J. X.; Trivette, A.; Nargi, R. S.; et al. Potently neutralizing and protective human antibodies against SARS-CoV-2. *Nature* **2020**, *584*, 443−449.

(9) Shi, R.; Shan, C.; Duan, X.; Chen, Z.; Liu, P.; Song, J.; Song, T.; Bi, X.; Han, C.; Wi, L.; et al. A human neutralizing antibody targets the receptor-binding site of SARS-CoV-2. *Nature* **2020**, *584*, 120−124.

(10) Liu, L.; Wang, P.; Nair, M. S.; Yu, J.; Rapp, M.; Wang, Q.; Luo, Y.; Chan, J. F-W.; Sahi, V.; Figueroa, A.; et al. Potent neutralizing antibodies against multiple epitopes on SARS-CoV-2 spike. *Nature* **2020**, *584*, 450−456.

(11) Sternberg, A.; Naujokat, C. Structural features of coronavirus SARS-CoV-2 spike protein: Targets for vaccination. *Life Sci.* **2020**, *257*, 118056.

(12) Dai, L.; Gao, G. F. Viral targets for vaccines against COVID-19. *Nat. Rev. Immunol.* **2021**, *21*, 73−82.

(13) Wang, Y.; Wang, L.; Cao, H.; Liu, C. SARS-CoV-2 S1 is superior to the RBD as a COVID-19 subunit vaccine antigen. *J. Med. Virol.* **2021**, *93*, 892−898.

(14) Irvine, D. J.; Read, B. J. Shaping humoral immunity to vaccines through antigen-displaying nanoparticles. *Curr. Opin. Immunol.* **2020**, *65*, 1−6.

(15) Shin, M. D.; Shukla, S.; Chung, Y. H.; Beiss, V.; Chan, S. K.; Ortega-Rivera, O. A.; Wirth, D. M.; Chen, A.; Sack, M.; Pokorski, J. K.; Steinmetz, N. F. COVID-19 vaccine development and a potential nanomaterial path forward. *Nat. Nanotechnol.* **2020**, *15*, 646−655.

(16) Singh, A. Eliciting B cell immunity against infectious diseases using nanovaccines. *Nat. Nanotechnol.* **2021**, *16*, 16−24.

(17) Tan, T. K.; Rijal, P.; Rahikainen, R.; Keeble, A. H.; Schimanski, L.; Hussain, S.; Harvey, R.; Hayes, J. W. P.; Edwards, J. C.; McLean, R. K.; et al. A COVID-19 vaccine candidate using SpyCatcher multimerization of the SARS-CoV-2 spike protein receptor-binding domain induces potent neutralising antibody responses. *Nat. Commun.* **2021**, *12*, 542.

(18) Kang, Y.-F.; Sun, C.; Zhuang, Z.; Yuan, R.-Y.; Zheng, Q.; Li, J.-P.; Zhou, P.-P.; Chen, X.-C.; Liu, Z.; Zhang, X.; et al. Rapid Development of SARS-CoV-2 Spike Protein Receptor-Binding Domain Self-Assembled Nanoparticle Vaccine Candidates. *ACS Nano* **2021**, *15*, 2738−2752.

(19) Walls, A. C.; Fiala, B.; Schäfer, A.; Wrenn, S.; Pham, M. N.; Murphy, M.; Tse, L. V.; Shehata, L.; O'Connor, M. A.; Chen, C.; et al. Elicitation of Potent Neutralizing Antibody Responses by Designed Protein Nanoparticle Vaccines for SARS-CoV-2. *Cell* **2020**, *183*, 1367−1382.e17.

(20) Cohen, A. A.; Gnanapragasam, P. N. P.; Lee, Y. E.; Hoffman, P. R.; Ou, S.; Kakutani, L. M.; Keeffe, J. R.; Wu, H.-J.; Howarth, M.; West, A. P.; et al. Mosaic nanoparticles elicit cross-reactive immune responses to zoonotic coronaviruses in mice. *Science* **2021**, *371*, 735−741.

(21) Jeyanathan, M.; Afkhami, S.; Smaill, F.; Miller, M. S.; Lichty, B. D.; Xing, Z. Immunological considerations for COVID-19 vaccine strategies. *Nat. Rev. Immunol.* **2020**, *20*, 615−632.

(22) Cox, R. J.; Brokstad, K. A. Not just antibodies: B cells and T cells mediate immunity to COVID-19. *Nat. Rev. Immunol.* **2020**, *20*, 581−582.

(23) Sette, A.; Crotty, S. Adaptive immunity to SARS-CoV-2 and COVID-19. *Cell* **2021**, *184*, 861−880.

https://doi.org/10.1021/acscentsci.1c00596
ACS Cent. Sci. 2021, 7, 1368−1380

(24) Chen, Z.; Wherry, E. J. T cell responses in patients with COVID-19. *Nat. Rev. Immunol.* **2020**, *20*, 529−536.
(25) Sekine, T.; Perez-Potti, A.; Rivera-Ballesteros, O.; Strålin, K.; Gorin, J.-B.; Olsson, A.; Llewellyn-Lacey, S.; Kamal, H.; Bogdanovic, G.; Muschiol, S.; et al. Robust T Cell Immunity in Convalescent Individuals with Asymptomatic or Mild COVID-19. *Cell* **2020**, *183*, 158−168.e14.
(26) Grifoni, A.; Weiskopf, D.; Ramirez, S. I.; Mateus, J.; Dan, J. M.; Moderbacher, C. R.; Rawlings, S. A.; Sutherland, A.; Premkumar, L.; Jadi, R. S.; et al. Targets of T Cell Responses to SARS-CoV-2 Coronavirus in Humans with COVID-19 Disease and Unexposed Individuals. *Cell* **2020**, *181*, 1489−1501.e15.
(27) Peng, Y.; Mentzer, A. J.; Liu, G.; Yao, X.; Yin, Z.; Dong, D.; Dejnirattisai, W.; Rostron, T.; Supasa, P.; Liu, C.; et al. Broad and strong memory CD4+ and CD8+ T cells induced by SARS-CoV-2 in UK convalescent individuals following COVID-19. *Nat. Immunol.* **2020**, *21*, 1336−1345.
(28) Bonifacius, A.; Tischer-Zimmermann, S.; Dragon, A. C.; Gussarow, D.; Vogel, A.; Krettek, U.; Gödecke, N.; Yilmaz, M.; Kraft, A. R. M.; Hoeper, M. M.; et al. COVID-19 immune signatures reveal stable antiviral T cell function despite declining humoral responses. *Immunity* **2021**, *54*, 340−354 e6.
(29) Diao, B.; Wang, C.; Tan, Y.; Chen, X.; Liu, Y.; Ning, L.; Chen, L.; Li, M.; Liu, Y.; Wang, G.; et al. Reduction and Functional Exhaustion of T Cells in Patients with Coronavirus Disease 2019 (COVID-19). *Front. Immunol.* **2020**, *11*, 827.
(30) Chen, G.; Wu, D.; Guo, W.; Cao, Y.; Huang, D.; Wang, H.; Wang, T.; Zhang, X.; Chen, H.; Yu, H.; et al. Clinical and immunological features of severe and moderate coronavirus disease 2019. *J. Clin. Invest.* **2020**, *130*, 2620−2629.
(31) Altmann, D. M.; Boyton, R. J. SARS-CoV-2 T cell immunity: Specificity, function, durability, and role in protection. *Sci. Immunol.* **2020**, *5*, eabd6160.
(32) Napoli, A.; Valentini, M.; Tirelli, N.; Müller, M.; Hubbell, J. A. Oxidation-responsive polymeric vesicles. *Nat. Mater.* **2004**, *3*, 183−189.
(33) Scott, E. A.; Stano, A.; Gillard, M.; Maio-Liu, A. C.; Swartz, M. A.; Hubbell, J. A. Dendritic cell activation and T cell priming with adjuvant- and antigen-loaded oxidation-sensitive polymersomes. *Biomaterials* **2012**, *33*, 6211−6219.
(34) Cerritelli, S.; O'Neil, C. P.; Velluto, D.; Fontana, A.; Adrian, M.; Dubochet, J.; Hubbell, J. A. Aggregation Behavior of Poly(ethylene glycol-bl-propylene sulfide) Di-and Triblock Copolymers in Aqueous Solution. *Langmuir* **2009**, *25*, 11328−11335.
(35) Stano, A.; Scott, E. A.; Dane, K. Y.; Swartz, M. A.; Hubbell, J. A. Tunable T cell immunity towards a protein antigen using polymersomes vs. solid-core nanoparticles. *Biomaterials* **2013**, *34*, 4339−4346.
(36) Galan-Navarro, C.; Rincon-Restrepo, M.; Zimmer, G.; Ollmann Saphire, E.; Hubbell, J. A.; Hirosue, S.; Swartz, M. A.; Kunz, S. Oxidation-sensitive polymersomes as vaccine nanocarriers enhance humoral responses against Lassa virus envelope glycoprotein. *Virology* **2017**, *512*, 161−171.
(37) Garçon, N.; Morel, S.; Didierlaurent, A.; Descamps, D.; Wettendorff, M.; Van Mechelen, M. Development of an AS04-Adjuvanted HPV Vaccine with the Adjuvant System Approach. *BioDrugs* **2011**, *25*, 217−226.
(38) Zhu, N.; Zhang, D.; Wang, W.; Li, X.; Yang, B.; Song, J.; Zhao, X.; Huang, B.; Shi, W.; Lu, R.; et al. A Novel Coronavirus from Patients with Pneumonia in China, 2019. *N. Engl. J. Med.* **2020**, *382*, 727−733.
(39) Stevens, T. L.; Bossie, A.; Sanders, V. M.; Fernandez-Botran, R.; Coffman, R. L.; Mosmann, T. R.; Vitetta, E. S. Regulation of antibody isotype secretion by subsets of antigen-specific helper T cells. *Nature* **1988**, *334*, 255−258.
(40) Chao, Y. X.; Rötzschke, O.; Tan, E.-K. The role of IgA in COVID-19. *Brain, Behav., Immun.* **2020**, *87*, 182−183.
(41) Renegar, K. B.; Small, P. A.; Boykins, L. G.; Wright, P. F. Role of IgA versus IgG in the control of influenza viral infection in the murine respiratory tract. *J. Immunol.* **2004**, *173*, 1978−1986.
(42) Hinton, D. M. *Convalescent Plasma EUA Letter of Authorization*, 2021.
(43) Yi, C.; Sun, X.; Ye, J.; Ding, L.; Liu, M.; Yang, Z.; Lu, X.; Zhang, Y.; Ma, L.; Gu, W.; et al. Key residues of the receptor binding motif in the spike protein of SARS-CoV-2 that interact with ACE2 and neutralizing antibodies. *Cell. Mol. Immunol.* **2020**, *17*, 621−630.
(44) Shang, J.; Ye, G.; Shi, K.; Wan, Y.; Luo, C.; Aihara, H.; Geng, Q.; Auerbach, A.; Li, F. Structural basis of receptor recognition by SARS-CoV-2. *Nature* **2020**, *581*, 221−224.
(45) Choi, Y. S.; Kageyama, R.; Eto, D.; Escobar, T. C.; Johnston, R. J.; Monticelli, L.; Lao, C.; Crotty, S. ICOS Receptor Instructs T Follicular Helper Cell versus Effector Cell Differentiation via Induction of the Transcriptional Repressor Bcl6. *Immunity* **2011**, *34*, 932−946.
(46) Akkaya, M.; Kwak, K.; Pierce, S. K. B cell memory: building two walls of protection against pathogens. *Nat. Rev. Immunol.* **2020**, *20*, 229−238.
(47) Toyama, H.; Okada, S.; Hatano, M.; Takahashi, Y.; Takeda, N.; Ichii, H.; Takemori, T.; Kuroda, Y.; Tokuhisa, T. Memory B Cells without Somatic Hypermutation Are Generated from Bcl6-Deficient B Cells. *Immunity* **2002**, *17*, 329−339.
(48) Mocellin, S.; Marincola, F. M.; Young, H. A. Interleukin-10 and the immune response against cancer: a counterpoint. *J. Leukocyte Biol.* **2005**, *78*, 1043−1051.
(49) Kishimoto, T. Interleukin-6: discovery of a pleiotropic cytokine. *Arthritis Res. Ther.* **2006**, *8*, S2.
(50) Cyster, J. G.; Allen, C. D. C. B Cell Responses: Cell Interaction Dynamics and Decisions. *Cell* **2019**, *177*, 524−540.
(51) Mesin, L.; Ersching, J.; Victora, G. D. Germinal Center B Cell Dynamics. *Immunity* **2016**, *45*, 471−482.
(52) Mohsen, M. O.; Zha, L.; Cabral-Miranda, G.; Bachmann, M. F. Major findings and recent advances in virus-like particle (VLP)-based vaccines. *Semin. Immunol.* **2017**, *34*, 123−132.
(53) Kato, Y.; Abbott, R. K.; Freeman, B. L.; Haupt, S.; Groschel, B.; Silva, M.; Menis, S.; Irvine, D. J.; Schief, W. R.; Crotty, S. Multifaceted Effects of Antigen Valency on B Cell Response Composition and Differentiation In Vivo. *Immunity* **2020**, *53*, 548−563 e8 (2020).
(54) Cyster, J. G. B cell follicles and antigen encounters of the third kind. *Nat. Immunol.* **2010**, *11*, 989−996.
(55) Catron, D. M.; Pape, K. A.; Fife, B. T.; van Rooijen, N.; Jenkins, M. K. A Protease-Dependent Mechanism for Initiating T-Dependent B Cell Responses to Large Particulate Antigens. *J. Immunol.* **2010**, *184*, 3609−3617.
(56) Phan, T. G.; Grigorova, I.; Okada, T.; Cyster, J. G. Subcapsular encounter and complement-dependent transport of immune complexes by lymph node B cells. *Nat. Immunol.* **2007**, *8*, 992−1000.
(57) Gonzalez, S. F.; Lukacs-Kornek, V.; Kuligowski, M. P.; Pitcher, L. A.; Degn, S. E.; Turley, S. J.; Carroll, M. C. Complement-Dependent Transport of Antigen into B Cell Follicles. *J. Immunol.* **2010**, *185*, 2659−2664.
(58) Carrasco, Y. R.; Batista, F. D. B Cells Acquire Particulate Antigen in a Macrophage-Rich Area at the Boundary between the Follicle and the Subcapsular Sinus of the Lymph Node. *Immunity* **2007**, *27*, 160−171.
(59) Oh, H. L. J.; Gan, S. K. E.; Bertoletti, A.; Tan, Y. J. Understanding the T cell immune response in SARS coronavirus infection. *Emerging Microbes Infect.* **2012**, *1*, 1−6.
(60) Shin, H.-S.; Kim, Y.; Kim, G.; Lee, J. Y.; Jeong, I.; Joh, J.-S.; Kim, H.; Chang, E.; Sim, S. Y.; Park, J.-S.; Lim, D.-G. Immune Responses to Middle East Respiratory Syndrome Coronavirus During the Acute and Convalescent Phases of Human Infection. *Clin. Infect. Dis.* **2019**, *68*, 984−992.
(61) Yasui, F.; Kai, C.; Kitabatake, M.; Inoue, S.; Yoneda, M.; Yokochi, S.; Kase, R.; Sekiguchi, S.; Morita, K.; Hishima, T.; et al. Prior Immunization with Severe Acute Respiratory Syndrome (SARS)-Associated Coronavirus (SARS-CoV) Nucleocapsid Protein Causes Severe Pneumonia in Mice Infected with SARS-CoV. *J. Immunol.* **2008**, *181*, 6337−6348.

https://doi.org/10.1021/acscentsci.1c00596
ACS Cent. Sci. 2021, 7, 1368−1380

(62) Liu, L.; Wei, Q.; Lin, Q.; Fang, J.; Wang, H.; Kwok, H.; Tang, H.; Nishiura, K.; Peng, J.; Tan, Z.; Wu, T.; et al. Anti-spike IgG causes severe acute lung injury by skewing macrophage responses during acute SARS-CoV infection. *JCI Insight* **2019**, *4*, No. e123158.
(63) Corbett, K. S.; Edwards, D. K.; Leist, S. R.; Abiona, O. M.; Boyoglu-Barnum, S.; Gillespie, R. A.; Himansu, S.; Schäfer, A.; Ziwawo, C. T.; DiPiazza, A. T.; et al. SARS-CoV-2 mRNA vaccine design enabled by prototype pathogen preparedness. *Nature* **2020**, *586*, 567−571.
(64) Vogel, A. B.; Kanevsky, I.; Che, Y.; Swanson, K. A.; Muik, A.; Vormehr, M.; Kranz, L. M.; Walzer, K. C.; Hein, S.; Güler, A.; et al. BNT162b vaccines protect rhesus macaques from SARS-CoV-2. *Nature* **2021**, *592*, 283−289.
(65) Casella, C. R.; Mitchell, T. C. Putting endotoxin to work for us: Monophosphoryl lipid A as a safe and effective vaccine adjuvant. *Cell. Mol. Life Sci.* **2008**, *65*, 3231−3240.
(66) Sallusto, F.; Cella, M.; Danieli, C.; Lanzavecchia, A. Dendritic cells use macropinocytosis and the mannose receptor to concentrate macromolecules in the major histocompatibility complex class II compartment: downregulation by cytokines and bacterial products. *J. Exp. Med.* **1995**, *182*, 389−400.
(67) Morón, V. G.; Rueda, P.; Sedlik, C.; Leclerc, C. In Vivo, Dendritic Cells Can Cross-Present Virus-Like Particles Using an Endosome-to-Cytosol Pathway. *J. Immunol.* **2003**, *171*, 2242−2250.
(68) Bachmann, M. F.; Jennings, G. T. Vaccine delivery: a matter of size, geometry, kinetics and molecular patterns. *Nat. Rev. Immunol.* **2010**, *10*, 787−796.
(69) Gamvrellis, A.; Leong, D.; Hanley, J. C.; Xiang, S. D.; Mottram, P.; Plebanski, M. Vaccines that facilitate antigen entry into dendritic cells. *Immunol. Cell Biol.* **2004**, *82*, 506−516.
(70) Panagioti, E.; Klenerman, P.; Lee, L. N.; van der Burg, S. H.; Arens, R. Features of effective T Cell-inducing vaccines against chronic viral infections. *Front. Immunol.* **2018**, *9*, 276.

https://doi.org/10.1021/acscentsci.1c00596
ACS Cent. Sci. 2021, 7, 1368−1380